Inorg. Chem. **2002**, *41*, 6583–6596

Distal Metal Effects in Cobalt Porphyrins Related to C*c*O

James P. Collman,* Katja E. Berg, Christopher J. Sunderland, Ally Aukauloo, Michael A. Vance, and Edward I. Solomon

Department of Chemistry, Stanford University, Stanford, California 94305-5080

Received June 12, 2002

Cobalt(II) porphyrins were studied to determine the influence of distal site metalation and superstructure upon dioxygen reactivity in active site models of cytochrome *c* oxidase (C*c*O). Monometallic, Co^{II}(P) complexes when ligated by an axial imidazole react with dioxygen to form reversible Co-superoxide adducts, which were characterized by EPR and resonance Raman (RR). Unexpectedly, certain Co porphyrins with Cu^{I} metalated imidazole pickets do not form μ-peroxo Co^{III}/Cu^{II} products even though the calculated intermetallic distance suggests this is possible. Instead, cobalt-porphyrin-superoxide complexes are obtained with the distal copper remaining as Cu^{I}. Moreover, distal metals (Cu^{I} or Zn^{II}) greatly enhance the stability of the dioxygen adduct, such that Co superoxides of bimetallic complexes demonstrate minimal reversibility. The "trapping" of dioxygen by a second metal is attributed to structural and electrostatic changes within the distal pocket upon metalation. EPR evidence suggests that the terminal oxygen in these bimetallic Co-superoxide systems is H-bonded to the NH of an imidazole picket amide linker, which may contribute to enthalpic stabilization of the dioxygen adduct. Stabilization of the dioxygen adduct in these bimetallic systems suggests one possible role for the distal copper in the Fe/Cu bimetallic active site of terminal oxidases, which form a heme-superoxide/copper(I) adduct upon oxygenation.

Introduction

Hemes (iron porphyrins) are widely used prosthetic groups for dioxygen transport and activation in biological systems.[1,2] Despite the absence of naturally occurring cobalt porphyrins, they have significantly added to the interpretation of heme protein-dioxygen chemistry. This contribution derives in part from the attenuated reactivity of the (P)CoO_2 (cobalt superoxide) unit compared to its heme counterpart, as manifested by a greater stability toward decomposition reactions. In addition, the single odd-electron configuration of d^7(P)Co(II) species allows EPR studies of the (P)Co(III)$O_2^{\bullet-}$ products, whereas (P)FeO_2 is EPR silent. This point is illustrated by the cobalt analogues of hemoglobin and myoglobin (CoHb, CoMb) and corresponding synthetic models.[3−5] Such studies have helped unravel the contributions of metal, porphyrin, proximal base, distal amino acid residue, and solvation to the binding and stabilization of heme-bound dioxygen.[1,6,7]

In cellular respiration, the reduction of dioxygen is mediated by terminal oxidases, such as cytochrome *c* oxidase (C*c*O).[8−10] At the active site of these enzymes is a highly conserved Fe/Cu (heme/trishistidyl-Cu) center at which dioxygen binding and reduction occurs. Extensive spectroscopic and crystallographic studies of C*c*O have illuminated many characteristics that lead to its efficient $4e^-$ reduction of dioxygen, although many controversial issues remain, especially concerning the role of Cu. Consequently, a number of synthetic Fe/Cu models have been prepared,[11−16] although

* To whom correspondence should be addressed. E-mail: jpc@stanford.edu. Fax 650-7250259.

(1) Jameson, G. B.; Ibers, J. A. In *Bioinorganic Chemistry*; Bertini, I., Gray, H. B., Lippard, S. J., Valentine, J. S., Eds.; University Science Books: Mill Valley, CA, 1994.
(2) Traylor, T. G.; Traylor, P. S. In *Active Oxygen in Biochemistry*; Valentine, J. S., Foote, C. S., Greenberg, A., Liebman, J. F., Eds.; Blackie Academic & Professional: London, 1995; Vol. 3, pp 84−187.
(3) Bruha, A.; Kincaid, J. R. *J. Am. Chem. Soc.* **1988**, *110*, 6006−6014.
(4) Proniewicz, L. M. K.; Kincaid, J. R. *J. Am. Chem. Soc.* **1990**, *112*, 675−681.
(5) Proniewicz, L. M. K.; Kincaid, J. R. *Coord. Chem. Rev.* **1997**, *161*, 81−127.
(6) Jones, R. D.; Summerville, D. A.; Basolo, F. *Chem. Rev.* **1979**, *79*, 139−179.
(7) Niederhoffer, E. C.; Timmons, J. H.; Martell, A. E. *Chem. Rev.* **1984**, *84*, 137−203.
(8) Capaldi, R. A. *Annu. Rev. Biochem.* **1990**, *59*, 569−596.
(9) Malmstrom, B. G. *Chem. Rev.* **1990**, *90*, 1247−1260.
(10) Ferguson-Miller, S.; Babcock, G. T. *Chem. Rev.* **1996**, *96*, 2889−2907.
(11) Tolman, W. B.; Spencer, D. J. E. *Curr. Opin. Chem. Biol.* **2001**, *5*, 188−195.
(12) Collman, J. P.; Fu, L.; Herrmann, P. C.; Wang, Z.; Rapta, M.; Broring, M.; Schwenninger, R.; Boitrel, B. *Angew. Chem., Int. Ed. Engl.* **1998**, *37*, 3397−3400.
(13) Collman, J. P.; Rapta, M.; Broring, M.; Raptova, L.; Schwenninger, R.; Boitrel, B.; Fu, L.; L'Her, M. *J. Am. Chem. Soc.* **1999**, *121*, 1387−1388.

10.1021/ic020395i CCC: $22.00
Published on Web 11/13/2002

Chart 1

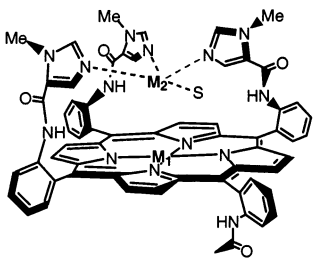

M_1 = Co: [Co**1**]
M_1 = Co, M_2 = Cu: [Co**1**Cu]

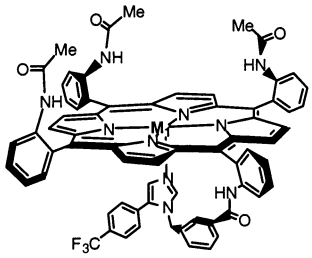

M_1 = Co: [Co**2**]

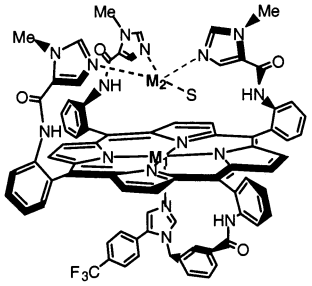

M_1 = Co: [Co**3**]
M_1 = Co, M_2 = Cu: [Co**3**Cu]

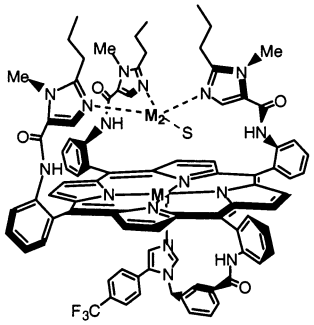

M_1 = Co: [Co**4**]
M_1 = Co, M_2 = Cu: [Co**4**Cu];
M_2 = Zn: [Co**4**Zn]; M_2 = Ag: [Co**4**Ag]

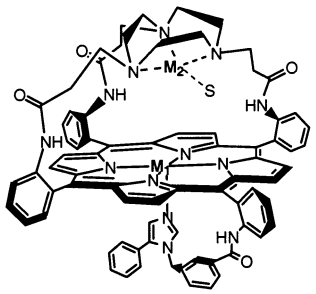

M_1 = Co: [Co**5**]
M_1 = Co, M_2 = Cu: [Co**5**Cu]

little kinetic and mechanistic information has been obtained because of the high reactivity and limited stability of these complexes. Despite the importance of simple picket and capped Co porphyrins to understanding hemoproteins, little progress has been made in extending such investigations to cobalt porphyrins which have distal ligand systems that provide covalently linked bimetallic Co/Cu complexes. The only published Co(porphyrin)/Cu C*c*O model was described by Collman in 1997 using a tetraphenylporphyrin system covalently linked to triazacyclononane (TACN).[17,18] A few examples of cobalt porphyrins having Ru, Zn, or Co in a distal amine structure have been reported with some spectroscopic characterization.[19−22] The synthesis of imidazole-picket porphyrins[23−25] (see Chart 1) provided an opportunity to study Co-porphyrin complexes that are chemically and structurally similar to the active site in C*c*O.

Herein we report the synthesis of a series of mono- and bimetallic (P)Co models having varying superstructural complexity and products deriving from their reaction with dioxygen. Benefiting from greater chemical stability and using resonance Raman (RR) and EPR spectroscopy, we have been able to define the starting (P)Co(II) species as well as their oxygenated adducts. The dioxygen affinities and characterization of the oxygen adducts reveal the effects of a distal metal (Cu, Zn, or Ag) on dioxygen binding. We propose that certain characteristics demonstrated by these compounds may be relevant to dioxygen chemistry in C*c*O.

Results and Discussion

Structure and Geometry. X-ray diffraction structures of the binuclear $Fe_{a3}-Cu_B$ active site in C*c*O have been determined for both bovine heart[26−28] and *Paracoccus denitrificans*,[29,30] revealing a trishistidyl ligated distal Cu

(14) Collman, J. P.; Schwenninger, R.; Rapta, M.; Broring, M.; Fu, L. *Chem. Commun.* **1999**, 137−138.
(15) Naruta, Y.; Sasaki, T.; Tani, F.; Tachi, Y.; Kawato, N.; Nakamura, N. *J. Inorg. Biochem.* **2001**, *83*, 239−246.
(16) Kopf, M.-A.; Karlin, K. D. In *Biomimetic Oxidations Catalyzed by Transition Metal Complexes*; Meunier, B., Ed.; Imperial College Press: London, 2000; pp 309−362.
(17) Collman, J. P.; Fu, L.; Herrmann, P. C.; Zhang, X. M. *Science* **1997**, *275*, 949−951.
(18) Collman, J. P. *Inorg. Chem.* **1997**, *36*, 5145−5155.
(19) Elliott, C. M.; Arnette, J. K.; Krebs, R. R. *J. Am. Chem. Soc.* **1985**, *107*, 4904−4911.
(20) Koeller, S.; Cocolios, P.; Guilard, R. *New J. Chem.* **1994**, *18*, 849−859.
(21) Kadish, K. M.; Shao, J. G.; Ou, Z. P.; Comte, C.; Gros, C. P.; Guilard, R. *J. Porphyrins Phthalocyanines* **2000**, *4*, 639−648.
(22) Andrioletti, B.; Ricard, D.; Boitrel, B. *New J. Chem.* **1999**, *23*, 1143−1150.
(23) Collman, J. P.; Broring, M.; Fu, L.; Rapta, M.; Schwenninger, R.; Straumanis, A. *J. Org. Chem.* **1998**, *63*, 8082−8083.
(24) Collman, J. P.; Broring, M.; Fu, L.; Rapta, M.; Schwenninger, R. *J. Org. Chem.* **1998**, *63*, 8084−8085.
(25) Collman, J. P.; Sunderland, C. J.; Boulatov, R. *Inorg. Chem.* **2002**, *41*, 2282−2291.
(26) Tsukihara, T.; Aoyama, H.; Yamashita, E.; Tomizaki, T.; Yamaguchi, H.; ShinzawaItoh, K.; Nakashima, R.; Yaono, R.; Yoshikawa, S. *Science* **1996**, *272*, 1136−1144.
(27) Yoshikawa, S.; ShinzawaItoh, K.; Nakashima, R.; Yaono, R.; Yamashita, E.; Inoue, N.; Yao, M.; Fei, M. J.; Libeu, C. P.; Mizushima, T.; Yamaguchi, H.; Tomizaki, T.; Tsukihara, T. *Science* **1998**, *280*, 1723−1729.
(28) Yoshikawa, S.; Shinzawa-Itoh, K.; Tsukihara, T. *J. Inorg. Biochem.* **2000**, *82*, 1−7.

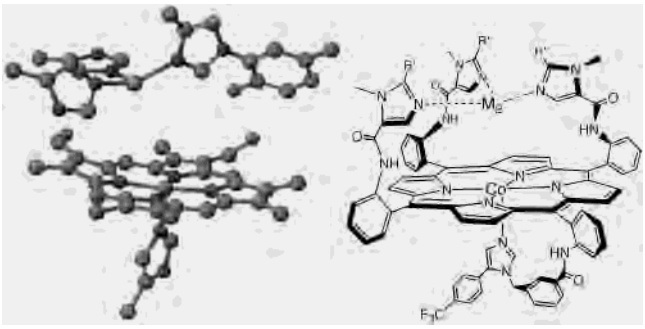

Figure 1. Comparison between the geometries of the active site of C*c*O (crystal structure from ref 28) and the designed (P)Co mimics.

placed about 4.5 Å above the Fe center in the heme (Figure 1). A proximal histidine is bound to Fe, and a redox-active tyrosine (Tyr244) extends from one of the distal histidine residues toward the catalytic pocket. To minimize synthetic efforts, earlier models of the active site made use of N-donor capping ligands (such as TACN, tpa, or tren) and exogenous proximal bases. Since the improved synthesis of $\alpha_3\beta$-picket phenylporphyrins in 1998,[23] a number of Fe/Cu porphyrins have been reported with this distinctive geometry.[31,32] Refining this concept to include covalently linked proximal imidazole and distal imidazole pickets, the ensuing model porphyrins closely mimic the structure of the C*c*O active site. These models were designed to evaluate the influence of the distal environment on ligand (O_2) binding. Previous results show differences in O_2 reactivity depending on the distal superstructure;[33,34] thus, we have chosen to examine a series of distal ligands, shown in Chart 1.

Synthesis and Metalation. The free base, Fe, Zn, Fe/Cu, and Zn/Cu complexes of α_3[imidazole]β[CF_3T] porphyrins **3** and **4** were prepared and characterized by Collman et al.[25] The α_3 geometry denotes three distal imidazole pickets, whereas β indicates a proximal axial imidazole ligand. For bimetallic porphyrins, the second metal of the pair (M_1/M_2) identifies the distal metal. In this work, Co and Co/Cu complexes of H_2**3** and H_2**4** have been investigated (see Scheme 1). Also, porphyrins with a β-acetylamide group H_2**1** as well as the α_3-acetamide picket porphyrin H_2**2** have been prepared. The imidazole-substituted free base porphyrins were found to be light sensitive. TACN-capped porphyrins such as **5** have been previously reported.[17,18]

Several methods have been reported for cobalt metalation of porphyrins.[35] Often, a cobalt(II) salt (e.g., Cl^-, AcO^-, NO_3^-) and a hindered base have been employed. In the present case, cobalt acetate was used to deprotonate and metalate the macrocycle without need for additional base, which was found to give product mixtures. Initial metalation of the pickets instead of the macrocycle was found in porphyrins with a secondary structure (**1**, **3**−**5**). Heating for an hour led to formation of the Co macrocycle, as indicated by a color change from purple-red to red-orange. Subsequent extraction utilizing aqueous EDTA removes the distal cobalt, leaving only the cobalt porphyrin in the organic phase. In earlier work, scrambling of the pickets was observed during metalation with cobalt under reflux.[36] To ensure that atropisomerization was not taking place, Zn metalation of the porphyrin was carried out under the same conditions. This reaction proceeded cleanly, yielding only the α_3-metalloporphyrin, as determined by TLC and ^{1}H NMR spectroscopy.

Several bimetallic complexes are reported herein. The combinations Co/Zn and Co/Ag have not previously been prepared. Whereas tetrahedral coordination of N-donor atoms to Zn(II) and Cu(I) is well-documented, only recently has the same preference been shown with silver in Ag(I) pyrazolylborate compounds.[37,38] The choice of solvent and counterion is important for introduction of the second metal. Usually, a 1-to-1 addition of a second metal to the metalloporphyrin was used with a solvent system (often mixtures of THF and MeOH) that is capable of dissolving the monometalated porphyrin, the metal salt, and the bismetalated product. To ensure better solubility and favor coordination to the distal pickets, metal triflates and hexafluorophosphates were used exclusively. Complete removal of the second metal was achieved by running the crude product through a column of aluminum oxide and/or by aq EDTA extraction. For [TACN]-capped systems, extraction of the second (distal) cobalt was achieved by addition of an excess of chelating amine (tetramethylethylenediamine) in THF and purification via chromatography. All mono- and bismetalated compounds are highly air-sensitive, and so, manipulation of these was carried out in a glovebox. Furthermore, certain combinations of metal oxidation states were observed to undergo redox reactions, even under an inert atmosphere (see later).

Spectroscopic Characterization. Several spectroscopic techniques were employed to determine the purity and homogeneity of these compounds prior to oxygen binding studies. The compositions of all Co metalated complexes were confirmed by ESI-MS and compared to calculated simulations of their isotope patterns. EPR spectroscopy was used to characterize these (d^7, $S = {}^1/_2$) Co(II) porphyrins. In every Co-only complex with an axial base, spectra typical of 5-coordinate Co(II) with axial symmetry were observed at 77 K, showing the expected hyperfine and superhyperfine coupling. In contrast to the commonly encountered 6-coordinate Co(III) porphyrin, (P)Co(II) usually exists as a 4- or 5-coordinate species.[35]

(29) Iwata, S.; Ostermeier, C.; Ludwig, B.; Michel, H. *Nature* **1995**, *376*, 660−669.
(30) Ostermeier, C.; Harrenga, A.; Ermler, U.; Michel, H. *Proc. Natl. Acad. Sci. U.S.A.* **1997**, *94*, 10547−10553.
(31) Ricard, D.; Didier, A.; L'Her, M.; Boitrel, B. *ChemBioChem* **2001**, *2*, 144−148.
(32) Collman, J. P.; Boulatov, R.; Sunderland, C. J. In *The Porphyrin Handbook*; Kadish, K. M., Smith, K., Guilard, R., Eds.; Academic Press: San Diego, CA; volume in press.
(33) Collman, J. P.; Fu, L. *Acc. Chem. Res.* **1999**, *32*, 455−463.
(34) Momenteau, M.; Reed, C. A. *Chem. Rev.* **1994**, *94*, 659−698.
(35) Sanders, J. K. M.; Bampos, N.; Clyde-Watson, Z.; Darling, S. L.; Hawley, J. C.; Kim, H.-J.; Ching Mak, C.; Webb, S. J. In *The Porphyrin Handbook*; Kadish, K. M., Smith, K. M., Guilard, R., Eds.; Academic Press: San Diego, CA, 2000; Vol. 3, p 23.
(36) Collman, J. P.; Zhang, X.; Wong, K.; Brauman, J. I. *J. Am. Chem. Soc.* **1994**, *116*, 6245−6251.
(37) Effendy, G.; Gioia Lobbia, G.; Pettinari, C.; Santini, C.; Skelton, B. W.; White, A. H. *Inorg. Chim. Acta* **2000**, *298*, 146−153.
(38) Rasika Dias, H. V.; Wang, Z.; Jin, W. *Inorg. Chem.* **1997**, *36*, 6205−6215.

Scheme 1. Synthetic Scheme of the Tris-imidazole Picketed Co and Co/Cu Porphyrins.

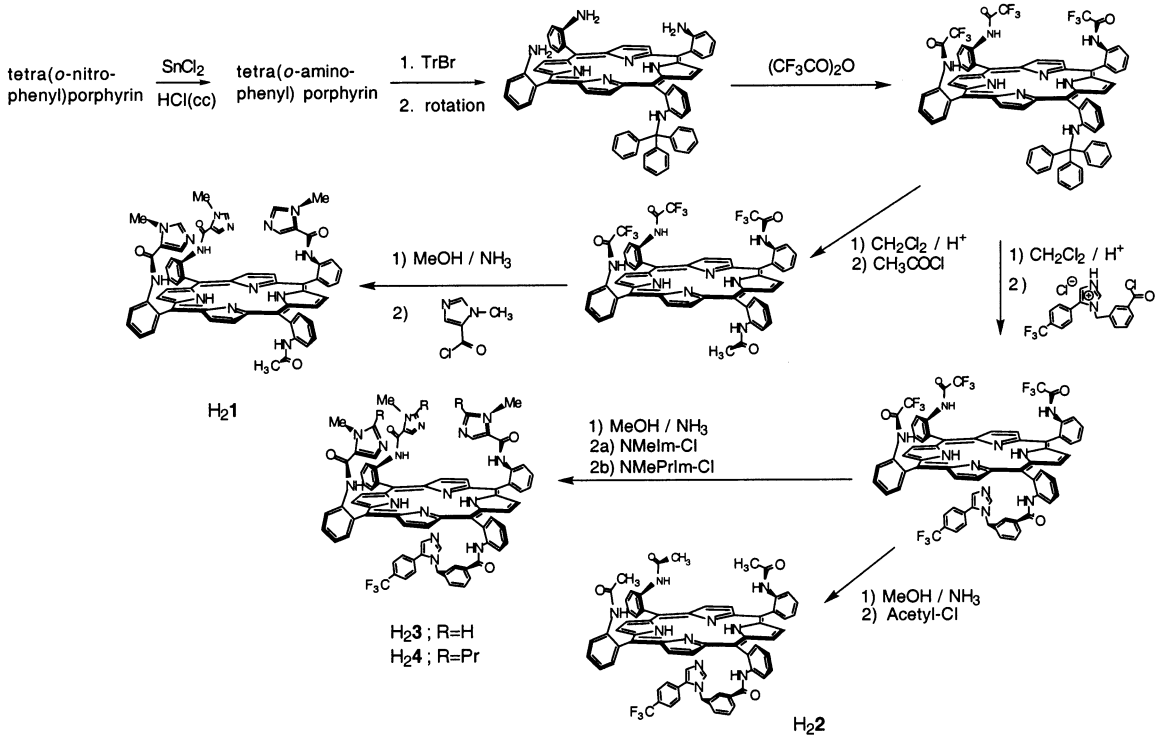

NMR spectroscopy was used to ensure purity and to gain insight into solution conformation. The paramagnetic Co(II) complex, [Co**3**], was oxidized to a diamagnetic Co(III) derivative, which was studied by NMR. Because of the low-spin d^7 configuration (unpaired electron in the d_{z^2} orbital), ^{1}H NMR spectra of Co(II) species yield broad signals.[39] In contrast to the planar and symmetric α_4-type Co(II) porphyrins,[40] each Co porphyrin reported here has complex distal and proximal superstructures resulting in broad signals and poorly resolved spectra. A CF_3-marker in the tail (axial base) portion of the porphyrin was included to monitor purity as well as to quantify Cu(I) binding. The latter was determined by integration of the porphyrin-bound CF_3-phenylimidazole against the F-containing copper counterion (hexafluorophosphate or triflate), using ^{19}F NMR spectroscopy. Upon oxidation of [Co**3**] to [Co**3**]$^+$, the ^{19}F signal of the paramagnetic species shifted from -66.84 to -67.60 ppm with narrowing of the line width at half-height to half of its previous value, as expected upon change to a diamagnetic species. Other ^{19}F NMR signals were not observed (Figure 2). The stereochemical homogeneity of [Co**3**]$^+$ was assayed using 1D and 2D ^{1}H NMR spectra. Interestingly, [Co**3**]$^+$ and [Fe**3**]CO (Co(III) is isoelectronic with low-spin Fe(II)) show similar chemical shift changes upon metalation of H_2**3**.[25] As shown in Figure 2, upfield shifted signals were found for the proximal imidazole and for the distal imidazole H4's, because of proximity to the porphyrin ring current. From this, it is concluded that the proximal imidazole is coordinated to cobalt and not exchanging in and out of the coordination sphere on the NMR time scale. This NMR spectrum also shows that the distal imidazole H4's point toward the porphyrin plane (with the imidazole *N*-methyl groups out). Therefore, in these Fe and Co cases, the relatively nonshifted Im$_\alpha$-H2's together with the upfield shifts of the Im$_\alpha$-H4's imply that the imidazole-(N3) lone pairs point into the cavity. For the Co porphyrin, the chemical shift change for Im$_\alpha$H4's (as compared to the free base) was 1.2 ppm upfield. The proximal Im$_\beta$-H2 and Im$_\beta$-H4 protons were observed to move 5−5.5 and 5.5−6.3 ppm upfield for the Fe(II)-CO and Co(III) adducts, respectively. We conclude that the gross structures of the picket imidazole porphyrins appear to be comparable regardless of the identity of the porphyrin metal.

It was important to establish insertion of Cu(I) into the distal site before evaluating oxygen binding. The presence of Cu(I) was evidenced by a combination of several techniques. EPR spectra of Co(II)/Cu(I) porphyrins have not been previously reported. Although Cu(I) (d^{10}, $S = 0$) is diamagnetic, small changes in the Co(II) *g*-values and hyperfine coupling were observed, probably because of electronic effects caused by copper (see Tables 2 and 3). When the Co(II)/Cu(I) species were subjected to 1 atm CO, typical CuC≡O IR stretching frequencies were observed. Conclusive ESI-MS ions were observed for the Co/Cu species and compared to the simulated copper-containing isotope patterns.

CO Binding. In dichloromethane solution, under an atmosphere of CO, [Co**1**Cu] and [Co**3**Cu] demonstrate CO stretching frequencies of 2085 and 2082 cm^{-1}, respectively (Table 1). These frequencies are consistent with carbon monoxide bound to a Cu(I) center, and with Cu having a tris-N donor (rather than a bis-N donor) environment. The coordination environment can be deduced from the frequency

(39) Walker, F. A. In *The Porphyrin Handbook*; Kadish, K. M., Smith, K. M., Guilard, R., Eds.; Academic Press: San Diego, CA, 2000; Vol. 5, pp 108, 160.
(40) Clayden, N. J.; Moore, G. R.; Williams, R. J. P.; Baldwin, J. E.; Crossley, M. J. *J. Chem. Soc., Perkin Trans. 2* **1983**, 1863−1868.

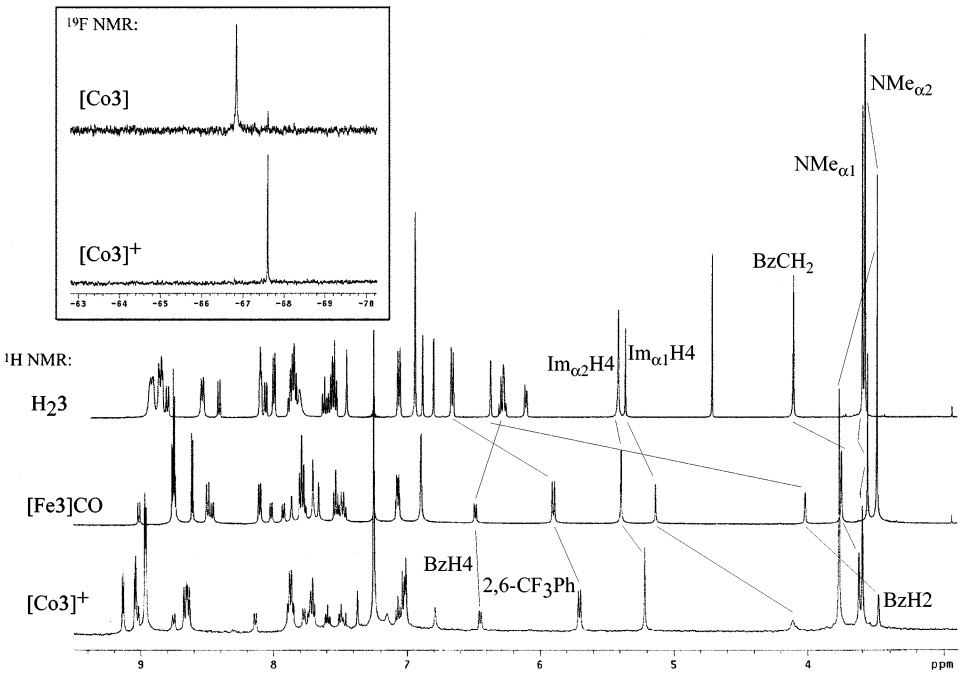

Figure 2. ^{1}H NMR spectra of **3**, recorded in $CDCl_3$ at RT. Free base (upper), Fe(II)CO (middle), and Co(III)X (lower). ^{19}F NMR spectra of Co(II) and Co(III) metalated **3** as an inset. Bz: protons of benzoyl tail linking the proximal imidazole to porphyrin. ImH4 or NMe α2 designation for mirror symmetric distal imidazole protons; α1 for unique central distal imidazole. Detailed assignments are in the Supporting Information.

Table 1. Infrared Stretching Frequencies for CO Bound in $Cu(I)(N)_3$ Chelates

complex	CuC−O stretch (cm^{-1})
[Co**3**Cu][a]	2082[h]
[Co**3**Cu][a]	2085[h]
[Co**4**Cu][a]	—[h]
[Fe**3**Cu][b]	2085[h]
[Fe**4**Cu][b]	—[h]
[Zn**3**Cu][b]	2087[h]
[Zn**4**Cu][b]	2079(w)[h]
$Cu(2\text{-MeIm})_3$[c]	2067[h]
$Cu[P(Im^{iPr_2})_3]$[d]	2083[h]
[Co**5**Cu][a]	2096[h]
[Fe**5**Cu][e]	2092(w)[h]
$Cu[Me_3TACN]$[f]	2020[i]
$Cu[^iPr_3TACN]$[g]	2067[i]
$Cu[Bn_3TACN]$[g]	2084[i]

[a] This work. [b] Reference 25. [c] Reference 82. [d] $P(Im^{iPr2})_3$ = tris[2-(1,4-diisopropylimidazoyl)]phosphine.[83] [e] Reference 84. [f] Reference 47. [g] Reference 48. [h] In CH_2Cl_2. [i] KBr pellet.

Table 2. EPR Parameters for 4- and 5-Coordinated Co and Co/Cu Species

porphyrin[a]	$g(x)$	$g(y)$	$g(z)$	$A_{\|}(^{59}Co)$ (mT)	$A_{\|}(^{14}N)$[d] (mT)
[Co**1**] (4-coord)	2.321	2.320	2.222		
[Co**1**]{NMeIm}$_{ax}$ (5-coord)	2.306	2.306	2.036	7.89	1.76
[Co**2**]	2.286	2.295	2.025	8.00	1.7
[Co**3**]	2.302	2.302	2.030	8.15	1.78
[Co**4**]	2.303	2.303	2.031	8.09	1.75
[Co**5**]	2.287	2.295	2.021	8.00	1.70
[Co**3**Cu]	2.291	2.303	2.031	8.00	1.7
[Co**4**Cu]	2.274	2.303	2.027	7.95	1.7
[Co**4**Ag]	2.302	2.302	2.032	7.70	1.70
[Co**4**Zn]	2.299	2.301	2.027	8.12	1.79
[Co**5**Cu]	2.293	2.287	2.022	8.01	1.73
CoMb[b] (5-coord conf by X-ray)	2.310	2.310	2.027	7.6	1.7
Co[T_{piv}PP]{NMeIm}$_{ax}$[c]	2.31	2.31	2.04	7.5	

[a] From this work, unless otherwise stated. Recorded in CH_2Cl_2 at 77 K. [*n*] = 2 mmol. X-band EPR. Simulations of EPR spectra performed with XSophe. [b] Reference 66. [c] Reference 64. [d] Number of decimals depends on the resolution of the hyperfine coupling.

of the vibration, because $(N)_2Cu-CO$ carbonyl stretches are observed to be >2110 cm^{-1}, whereas a range 1950−2100 cm^{-1} has been observed for a number of $(N)_3CuCO$ complexes.[41] Additionally, these ν(CO) values are consistent with those of [Fe**3**Cu]CO and [Zn**3**Cu]CO, which display stretches at 2085 and 2087 cm^{-1}, respectively.[25] In all cases (Fe/Cu, Zn/Cu or Co/Cu), CO binding to copper is reversible. Formation of a CO adduct was not observed for the Co-only complexes. This observation, along with the appearance of only a single carbonyl stretch and the similarity to ν(CO) of [Fe**3**Cu]CO, supports the conclusion that CO is not binding to the Co(II) center, although CO binding has been observed in some Co(II) porphyrins at low temperatures.[42−44] By contrast, cobalt(III) porphyrins bind CO readily.[45,46]

[Co**4**Cu] does not bind carbon monoxide at 1 atm CO pressure, as was noted for the corresponding Fe porphyrin. It was suggested that a steric effect from the propyl groups at the 2-position of NMePrIm leads to decreased affinity for CO at the Cu-imidazole site.[25] Thus, it appears that the copper environment in Co(II)/Cu(I) metalated **3** and **4** is similar to that claimed for the corresponding Fe(II)/Cu(I) and Zn(II)/Cu(I) complexes. We conclude, as depicted in Figure 1, that

(41) Rondelez, Y.; Seneque, O.; Rager, M. N.; Duprat, A. F.; Reinaud, O. *Chem. Eur. J.* **2000**, *6*, 4218−4226 and references therein.
(42) Wayland, B. B.; Minkiewixz, J. V.; Abd-Elmageed, M. E. *J. Am. Chem. Soc.* **1974**, *96*, 2795−2801.
(43) Wayland, B. B.; Sherry, A. E.; Bunn, A. G. *J. Am. Chem. Soc.* **1993**, *115*, 7675−7684.
(44) Kozuka, M.; Nakamoto, K. *J. Am. Chem. Soc.* **1981**, *103*, 2162−2168.
(45) Schmidt, E.; Zhang, H.; Chang, C. K.; Babcock, G. T.; Oertling, W. A. *J. Am. Chem. Soc.* **1996**, *118*, 2954−2961.
(46) Kadish, K. M.; Li, J.; Van Caemelbecke, E.; Ou, Z. P.; Guo, N.; Autret, M.; F, D. S.; Tagliatesta, P. *Inorg. Chem.* **1997**, *36*, 6292−6298.

Table 3. EPR Parameters for Oxygenated Co and Co/Cu Species.

porphyrin[a]	$g(x)$	$g(y)$	$g(z)$	a_1 (mT)	a_2 (mT)	a_3 (mT)
[CoTPP]{NMeIm}$_{ax}O_2$[b]	2.083	2.004	1.985	2.1	0.5	0.4
[Co**2**]{NMeIm}$_{ax}O_2$	2.083	2.002	1.995	1.7	1.1	0.6
[Co**2**]O_2	2.081	2.004	1.981	1.7[c]	1.1[c]	1.0[c]
[Co**3**]O_2	2.084	2.005	1.991	1.7[c]	1.1[c]	0.9[c]
[Co**4**]O_2	2.077	2.003	1.986	1.7[c]	1.1[c]	0.9[c]
[Co**5**]O_2	2.072	1.998	1.985	1.7[c]	1.1[c]	0.9[c]
[Co**3**Cu]O_2	2.082	2.007	1.986	1.71	1.0	0.9
[Co**4**Cu]O_2	2.084	2.006	1.993	1.71	1.0	1.0
[Co**4**Ag]O_2	2.082	2.002	1.987	1.68	1.03	0.86
[Co**4**Zn]O_2	2.084	2.007	1.990	1.68	0.98	0.83
$CoMbO_2$ (Type 1)[d]	2.08	2.03	1.98	2.32	0.62	0.72
$CoMbO_2$ (Type 2)[d]	2.085	2.008	1.983	1.73	0.82	0.77
[CoT_{piv}PP]{NMeIm}$_{ax}O_2$[e]	2.09 (∥)	2.01 (⊥)		2.0		

[a] From this work, unless otherwise stated. Recorded in CH_2Cl_2 at 77 K. [*n*] = 2 mmol. X-band EPR. Simulations of EPR spectra performed with XSophe. [b] Reference 67. [c] Nonresolved hyperfine. [d] Reference 85. [e] Reference 64.

the distal copper appears to be in a tris-imidazole coordination sphere above the porphyrin plane.

For [Co**5**Cu]CO, ν(CO) was observed at 2096 cm^{-1} (1 atm CO/CH_2Cl_2). As for the imidazole-picket porphyrins discussed earlier in the text, CO binding to Cu is reversible. While the CO stretch is within the range associated with $(N)_3$CuCO species, it is somewhat higher than the highest frequency reported to date for (R_3TACN)CuCO complexes (2020−2092 cm^{-1}).[47−50] Higher ν(CO) values indicate weakened metal-to-CO back-bonding. The CO frequency of (R_3TACN)CuCO species demonstrates dependence on electron donation from the R-groups as well as differences due to steric-induced structural changes. The high CO stretching frequency of [Co**5**Cu]CO may partly be from decreased N-donor basicity due to the electron-withdrawing amido (tethering) substituents. Given the location of the TACN above the porphyrin ring, distortion of the Cu−CO bonding due to conformational constraints at the TACN, and steric interaction with the porphyrin ring, may also be contributing factors. Transfer of electron density onto the CO may also be diminished because of electrostatic interaction of the M-CO oxygen with the porphyrin π system or other lone pairs, a phenomenon observed with heme-CO complexes,[51−55] but not systematically studied in copper-CO complexes.

Oxygen Binding. Throughout the catalytic cycle in C*c*O, Cu_B is subjected to changes in oxidation state and coordination geometry. Along this cycle, a peroxide state [Fe(III)−O_2···Cu(II)]$^+$ (P-state) has been suggested, but little evidence supports this theory.[56,57] If the peroxide state is formed, it exists as a short-lived intermediate or in small amounts, difficult to detect. Nonetheless, formation of peroxides has been observed for Fe/Cu models.[12,17,58−63] Usually, this is found for Fe/Cu models where the donor ability and geometry of the capping ligand are able to stabilize Cu(II), favoring formation of a peroxide intermediate. Similar reactivity was expected for the α_3[imidazole]β[imidazole] porphyrins. As a first spectroscopic assessment of oxygen reactivity with these complexes, a choice of cobalt over iron was made to gain kinetic and product stability. Little information on cobalt porphyrin models of C*c*O exists as only two types of superstructured (and bimetallic) Co-porphyrins have been reported.[18,22] Upon oxygenation, our Co-only porphyrins reversibly form Co superoxides. Because our efforts were targeted toward understanding the bimetallic structure−function relationships in C*c*O, and especially the role of copper, a redox-active copper was introduced into the pickets of the cobalt complexes of **1**, **3**, and **4**. Hitherto, in the sole Co/Cu porphyrin system studied, [Co**5**Cu], a stable Co−O_2−Cu peroxide bridge was formed (ν(O−O) = 802 cm^{-1}; $\Delta\nu(^{16}O_2-^{18}O_2)$ = 48 cm^{-1}).[18] Peroxide formation has also been reported for a cyclam-strapped Co/Co porphyrin, yielding a stable Co−O_2−Co adduct.[22]

Co and Co/Cu Porphyrins before Oxygenation. The EPR spectrum of the 4-coordinated Co(II) porphyrin [Co**1**] ($g_{\|}$ = 2.22, $g_{\perp}$ = 2.32) shows neither hyperfine nor superhyperfine structure (examples of EPR spectra for various coordinations are shown in Figure 3). Introduction of a base (NMeIm) alters the electron distribution (especially in the parallel direction to the field), and coupling is observed (Table 2). A decrease in $g_{\|}$ (∼2.03) and the appearance of hyperfine ($A_{\|}(^{59}Co)$ ∼8 mT) as well as superhyperfine ($A_{\|}(^{14}N)$ ∼1.7−1.8 mT) couplings were monitored. The resulting EPR spectrum of {NMeIm}$_{ax}$[Co**1**] displays axial symmetry, characteristic of a 5-coordinate Co(II) complex with a nitrogenous base axial ligand parallel to the magnetic field ($g_{\|}$). Because of interaction between ^{59}Co ($I = {}^7/_2$) and ^{14}N ($I = 1$), an octet hyperfine structure with a triplet superhyperfine coupling pattern is observed, ruling out a second coordinated base even at large excess of NMeIm. Previous studies of cobalt(II) porphyrins and NMeIm as base have never demonstrated double occupancy of the axial positions.[35]

(47) Chaudhuri, P.; Oder, K. *J. Organomet. Chem.* **1989**, *367*, 249−258.
(48) Mahapatra, S.; Halfen, J. A.; Wilkinson, E. C.; Pan, G. F.; Wang, X. D.; Young, V. G.; Cramer, C. J.; Que, L.; Tolman, W. B. *J. Am. Chem. Soc.* **1996**, *118*, 11555−11574.
(49) Berreau, L. M.; Halfen, J. A.; Young, V. G.; Tolman, W. B. *Inorg. Chem.* **1998**, *37*, 1091−1098.
(50) Berreau, L. M.; Halfen, J. A.; Young, V. G.; Tolman, W. B. *Inorg. Chim. Acta* **2000**, *297*, 115−128.
(51) Park, K. D.; Guo, K.; Adebodun, F.; Chiu, M. L.; Sligar, S. G.; Oldfield, E. *Biochemistry* **1991**, *30*, 2333−2347.
(52) Ray, G. B.; Li, X. Y.; Ibers, J. A.; Sessler, J. L.; Spiro, T. G. *J. Am. Chem. Soc.* **1994**, *116*, 162−176.
(53) Uno, T.; Mogi, T.; Tsubaki, M.; Nishimura, Y.; Anraku, Y. *J. Biol. Chem.* **1994**, *269*, 11912−11920.
(54) Spiro, T. G.; Kozlowski, P. M. *Acc. Chem. Res.* **2001**, *34*, 137−144.
(55) Rovira, C.; Schulze, B.; Eichinger, M.; Evanseck, J. D.; Parrinello, M. *Biophys. J.* **2001**, *81*, 435−445.
(56) Proshlyakov, D. A.; Pressler, M. A.; Babcock, G. T. *Proc. Natl. Acad. Sci. U.S.A.* **1998**, *95*, 8020−8025.
(57) Fabian, M.; Wong, W. W.; Gennis, R. B.; Palmer, G. *Proc. Natl. Acad. Sci. U.S.A.* **1999**, *96*, 13114−13117.
(58) Collman, J. P.; Herrmann, P. C.; Boitrel, B.; Zhang, X. M.; Eberspacher, T. A.; Fu, L.; Wang, J. L.; Rousseau, D. L.; Williams, E. R. *J. Am. Chem. Soc.* **1994**, *116*, 9783−9784.
(59) Sasaki, T.; Nakamura, N.; Naruta, Y. *Chem. Lett.* **1998**, 351−352.
(60) Ghiladi, R. A.; Ju, T. D.; Lee, D. H.; Moenne-Loccoz, P.; Kaderli, S.; Neuhold, Y. M.; Zuberbuhler, A. D.; Woods, A. S.; Cotter, R. J.; Karlin, K. D. *J. Am. Chem. Soc.* **1999**, *121*, 9885−9886.
(61) Kopf, M. A.; Neuhold, Y. M.; Zuberbuhler, A. D.; Karlin, K. D. *Inorg. Chem.* **1999**, *38*, 3093−3102.
(62) Kopf, M. A.; Karlin, K. D. *Inorg. Chem.* **1999**, *38*, 4922−4923.
(63) Ghiladi, R. A.; Hatwell, K. R.; Karlin, K. D.; Huang, H. W.; Moenne-Loccoz, P.; Krebs, C.; Huynh, B. H.; Marzilli, L. A.; Cotter, R. J.; Kaderli, S.; Zuberbuhler, A. D. *J. Am. Chem. Soc.* **2001**, *123*, 6183−6184.

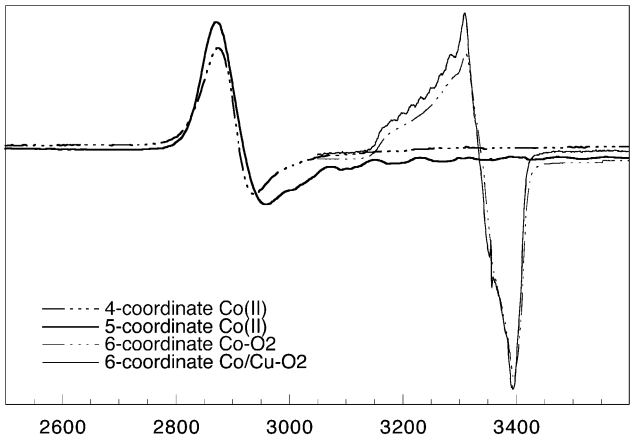

Figure 3. Examples of EPR spectra for 4-, 5-, and 6-coordinated species.

However, it is possible that a coordinating solvent molecule, such as water, might be retained inside the distal pocket and held within this cavity by weak coordination to cobalt and/or hydrogen bonding. In earlier studies of picket fence cobalt porphyrins with excess NMeIm, an exclusively proximal substitution of the exogenous base was suggested, explained by the steric hindrance of the *tert*-butyl pickets.[36,64] It is also likely that, in [Co**1**], distal axial ligation is suppressed by the steric bulk of the imidazoles, although binding in the cavity cannot be excluded.

All estimated *g*-values and coupling constants obtained from simulations of the recorded EPR spectra are consistent with literature values for Co-porphyrin models as well as for cobalt-substituted enzymes, for example, cobalt heme oxygenase,[65,66] cobalt hemoglobin,[67] and cobalt myoglobin[68] (Table 2). EPR spectra of [Co**2**], [Co**3**], and [Co**4**] are each consistent with 5-coordinate cobalt having one Co-bound imidazole (the endogenous CF_3T tail). The presence of Cu(I), Ag(I), or Zn(II) in the distal pocket causes some changes in *g* values, especially in $g_\perp$, and/or in hyperfine coupling. The presence of Cu(I), for example, appears to induce a higher degree of anisotropy ($g_\perp$) together with a decrease in $A_{||}$ (^{59}Co). Broadening of this signal was observed, possibly because of a bridging solvent or simply reshuffling of the electronic distribution due to the presence of a positive metal center in the cap.

Co−O_2 Complexes. When 5-coordinate Co(II) porphyrins are exposed to oxygen, large changes in *g*-values and coupling constants are observed. Simulations of the EPR spectra indicated free-radical-like signals ($g \sim 2$) and smaller $A_{||}$ (^{59}Co) (∼1.7 mT) (Table 3). This feature is characteristic of monomeric cobalt porphyrins having one O_2 molecule bound in a bent end-on fashion, formally denoted as Co(III)−$O_2^{\bullet-}$.[69] Because [Co**3**] and [Co**4**] (endogenous bases) show 5-coordinated cobalt prior to oxygenation, the O_2 in the Co-superoxo species is most likely located inside the distal cavity (and likewise for {NMeIm}$_{ax}$[Co**1**]), as has previously been shown for α_4 picket fence Co porphyrins.[36,64] All Co-superoxo porphyrins herein are consistent with literature values of a B−Co(P)−O_2 core,[6] as demonstrated in Table 3. All EPR samples were examined by ESI-MS to confirm the formation of Co−oxy species. The molecular peaks for the Co−O_2 parent ions were weak, but Co−O_2 peaks were observed for the following compounds: {NMeIm}$_{ax}$[Co**1**]O_2 = 1235 (30%), [Co**2**]O_2 = 1217 (18%), [Co**3**]O_2 = 1417 (3%).

Oxygenation of [Co**3**Cu] and [Co**4**Cu] (1 atm O_2) gave an unexpected result. Instead of the anticipated Cu(II) signal of a Co−O_2−Cu species (with the unpaired electron on copper), an EPR spectrum characteristic of a Co-superoxo species was observed (Table 3). At lower concentrations of oxygen (to slow oxygenation), overlapping signals of Co-superoxo and Co-only species were detected. Cu(II) was never observed, even when the oxygenation was quenched immediately after addition of oxygen by freezing the sample to 77 K. No EPR evidence for a peroxo-bridged species was seen.

The capacity of the three imidazole pickets to coordinate Cu(II) was studied. Generally, copper(II) ($S = {}^1/_2$, $I = {}^3/_2$) gives characteristic spectra where the positions of $g_{||}$ versus $g_\perp$ indicate the geometry of Cu(II) and the (super)hyperfine coupling suggests the number and nature of the coordinated atoms.[70] $CuTf_2$ was titrated into the diamagnetic [Co**3**]$^+$ porphyrin, and a signal typical for square planar (or pyramidal) Cu(II) was obtained, although it was poorly resolved. However, addition of $CuTf_2$ to [Zn**3**] resulted in a well-resolved spectrum characteristic of Cu(II) in a square planar arrangement where $g_{||} = 2.281$, $g_\perp = 2.053$, and $A_{||}$(Cu) = 16.5 mT. The superhyperfine coupling pattern of the $g_\perp$ signal ($A_{||}(^{14}N)$=1.5 mT) is consistent with at least 3 nitrogen donor atoms coupled to copper. A similar spectrum was obtained for the previously reported [Zn**3**Cu^{II}Cl] ($g_{||}$ = 2.28, $g_\perp = 2.07$, $A_{||}$(Cu) = 17.5 mT, $A_{||}(^{14}N)$ = 1.5 mT, $A_\perp$ = 1.3 mT).[25] Free Cu(II) triflate ($g_{||} = 2.344$ and $g_\perp = 2.073$, $A_{||}$(Cu) = 14.6 mT) was not observed in the M_1/Cu(II) samples.

Reversibility. Generally, cobalt-O_2 porphyrins show complete or partial reversibility upon either purging, pumping, heating, or irradiating the complex.[36,71] According to earlier reports,[72] at low temperatures Co−O_2 equilibria are shifted in favor of the Co−O_2 complex. The Co-only systems reported herein bind dioxygen reversibly at RT as demonstrated in the EPR spectra shown in Figure 5. [Co**4**] placed under oxygen for 2 h gave a spectrum of coexisting Co-only and Co−O_2. The same sample held for 1.5 h under vacuum at RT yielded >90% Co-only. After 15 h under

(64) Collman, J. P.; Brauman, J. I.; Doxsee, K. M.; Halbert, T. R.; Hayes, S. E.; Suslick, K. S. *J. Am. Chem. Soc.* **1978**, *100*, 2761−2766.
(65) Chu, G. C.; Tomita, T.; Sonnichsen, F. D.; Yoshida, T.; Ikeda-Saito, M. *J. Biol. Chem.* **1999**, *274*, 24490−24496.
(66) Fujii, H.; Dou, Y.; Zhou, H.; Yoshida, T.; Ikeda-Saito, M. *J. Am. Chem. Soc.* **1998**, *120*, 8251−8252.
(67) Bowen, J. H.; Shokhirev, N. V.; Raitsimring, A. M.; Buttlaire, D. H.; Walker, F. A. *J. Phys. Chem. B* **1997**, *101*, 8683−8691.
(68) Brucker, E. A.; Olson, J. S.; Phillips, G. N.; Dou, Y.; Ikeda-Saito, M. *J. Biol. Chem.* **1996**, *271*, 25419−25422.
(69) VanDoorslaer, S.; Bachmann, R.; Schweiger, A. *J. Phys. Chem. A* **1999**, *103*, 5446−5455.
(70) Hathaway, B. J. *Comprehensive Coordination Chemistry*; Pergamon Press: New York, 1987; Vol. 5.
(71) Walker, F. A. *J. Am. Chem. Soc.* **1970**, *92*, 4235−4244.
(72) Salmon, L.; Biedcharreton, C.; Gaudemer, A.; Moisy, P.; Bedioui, F.; Devynck, J. *Inorg. Chem.* **1990**, *29*, 2734−2740.

oxygen, this equilibrium went to 100% completion; subsequent removal of the oxygen head-gas regenerated the 5-coordinate Co(II) porphyrin. Because of some background oxidation that forms a Co(III)−X adduct over time (indistinguishable from Co superoxide by UV−vis spectroscopy), quantitative equilibrium constants could not be obtained. In the higher concentrations used with EPR experiments (mM), this oxidation process is insignificant, as compared to the low-concentration UV−vis measurements (μM).

$$[\text{Co(II)Por}][\text{B}] + \text{O}_2 \rightleftharpoons [\text{Co(III)Por}][\text{B}]\text{O}_2^{\bullet-} \qquad (1)$$

The final products obtained from reaction of O_2 with Co/Cu, Co/Ag, and Co/Zn complexes each showed spectra characteristic of a Co superoxide, with well-resolved hyperfine features (Figure 4). All these oxygenations were seemingly irreversible, which would have been expected for peroxide-bridged but not superoxide-type complexes.

$$[\text{Co(II)/Cu(I)Por}][\text{B}] + \text{O}_2 \rightleftharpoons [\text{Co(III)/Cu(I)Por}][\text{B}]\text{O}_2^{\bullet-} \qquad (2)$$

Interestingly, the [Co**2**] complex shows reversible O_2 binding, but with a higher dioxygen affinity than the imidazole-picket Co-only porphyrins of **1**, **3**, and **4**. Oxygen affinity studies have shown that, in porphyrin models where amides or other groups capable of H-bonding are bound close to the coordinated oxygen, a large increase in oxygen affinity is observed.[36,73] This enhancement was accounted for by H-bonding and/or dipole−dipole interaction in the cavity, which has also been demonstrated by other groups.[65,66,74] As the O_2 molecule binds to the Co(II) center, the complex formally written as Co(III)−$O_2^{\bullet-}$ has a strong dipole,[69] where Co(III) is in a low-spin d^6 state and the electronegative terminal oxygen of the superoxide may additionally be stabilized by neighboring δ^+ charges. We propose that the high oxygen affinity observed for the Co/Cu complexes may be due to conformational changes in the distal superstructure upon metalation of the picket imidazoles and/or electrostatic effects caused by the presence of the second metal. Correspondingly, high oxygen affinity was found for the Co/Zn species. In contrast, the imidazole lone pairs (δ^- charge) in the Co-only complexes are directed into the cavity and may destabilize the superoxide adduct. It should be noted that simple Co porphyrins function as O_2 carriers similar to Mb and Hb, whereas the superstructured Co/Cu porphyrins retain the O_2 molecule in the active site, paralleling characteristics of bimetallic C*c*O where O_2 is retained for reduction. Electrochemical potentials and catalytic reductions of these C*c*O analogues will be discussed in a following paper.

H-Bonding. Oxygenation of the Co-only complexes [Co**3**] and [Co**4**] leads to EPR spectra with poorly resolved hyperfine coupling. This phenomenon may be explained either as superimposed Co-superoxo signals originating from a mixture of frozen Co-superoxide conformations, or by a freely rotating O_2-unit in the distal cavity. When distal Cu(I) is

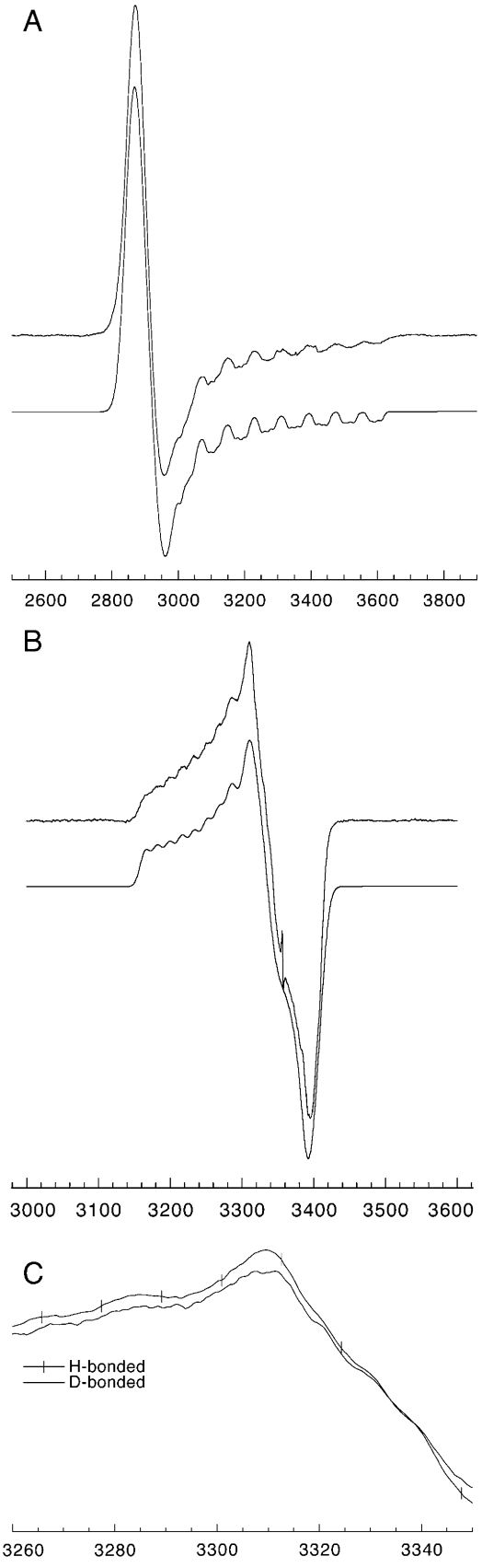

Figure 4. Examples of experimental EPR spectra (upper trace) and simulations (lower trace) of [Co**4**] (A) and [Co**4**Cu]O_2 (B) porphyrins. H vs D experiment for [Co**4**Cu]O_2 (C).

(73) Tang, H.; Dolphin, D. *Inorg. Chem.* **1996**, *35*, 6539−6545.
(74) Chu, G. C.; Tomita, T.; Sonnichsen, F.; Yoshida, T.; Ikeda-Saito, M. *Biophys. J.* **1999**, *76*, A426−A426.

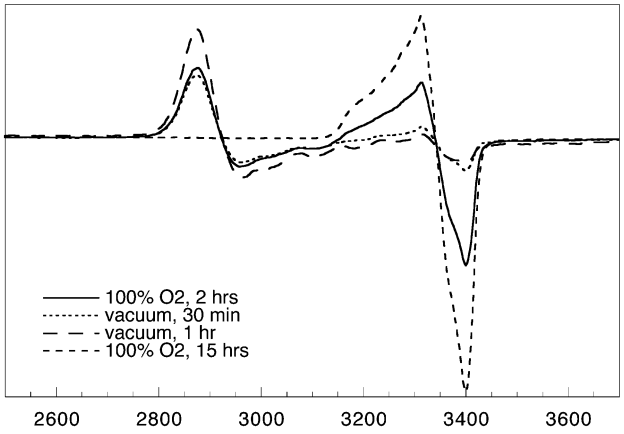

Figure 5. Demonstrated reversibility of O_2 binding for the Co-only porphyrin [Co**4**].

present and the bimetallic complexes are oxygenated, an EPR spectrum with resolved hyperfine coupling was observed. Walker and Bowen investigated hydrogen bond donation from neighboring acetamides to the terminal oxygen in Co−O_2 porphyrins.[67,75] Enthalpic stabilization due to the amide N−H bonding to bound O_2 was shown to depend on the substitution position of the acetamide (*ortho* vs *para*). This effect was observed as a loss or appearance of hyperfine coupling in the spectra of various Co−O_2 adducts as a function of temperature. At low temperatures, an *ortho*-acetamide H-bonds to O_2, locking that conformation and giving rise to hyperfine coupling, which is lost at elevated temperatures. With a *para*-acetamide substitution where such H-bonding to O_2 is not possible, an almost completely motionally averaged EPR spectrum is observed, consistent with the oxygen molecule freely rotating about the Co−O bond.

A paramagnetic center surrounded by ions with nuclear magnetic moments, such as protons, experiences magnetic dipole−dipole interactions leading to spectral line broadening. In comparison to the proton, the smaller nuclear magnetic moment of deuterium may reduce the line width by a factor of 33%. If exchangeable protons are near the paramagnetic Co−O_2 center, a deuterated environment should result in reduction of the line width yielding a sharpened hyperfine structure. For the oxy-Co analogues of heme oxygenase and a related heme degradation enzyme Hmu O,[65,66] H-bonding to a neighboring amide was examined by H/D exchange experiments. Comparison of the EPR spectra of the H and D systems revealed different coupling patterns for the Co-superoxide signals. Specifically, hyperfine coupling was found to be more pronounced in the D experiments. Similarly, in the present studies, differences in the hyperfine coupling of H- and D-substituted amides were observed for both [Co**4**Cu]O_2 (Figure 4C) and [Co**4**Zn]O_2 complexes, whereas no change was seen in an analogous experiment using [Co**4**]O_2.

In conclusion, O_2 appears to be freely rotating in the [Co**3**]-O_2 and [Co**4**]O_2 complexes. The Co/Cu and Co/Zn complexes of both porphyrins demonstrate evidence for H-bonding, which may be explained as Co-superoxide signals manifesting hindered oxygen rotations due to H-bonding to the amide and/or the imposed tighter distal pocket structure when Cu or Zn is present to assemble the capping imidazoles (Figure 6).

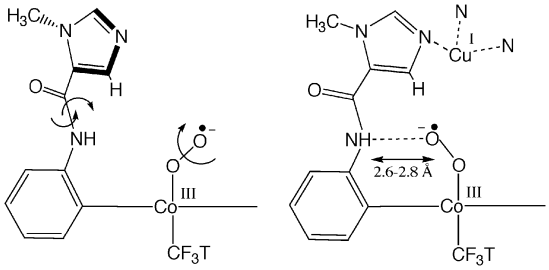

Figure 6. Illustration of plausible H-bonding in the cavity.

Parameters for the imidazole pickets of a zinc α_4[NMeIm] structure[76] combined with parameters for the Co-superoxo core from the solved CoMb structure[68] were utilized in molecular mechanics calculations (MM3; MM3 minimization performed with software program CAChe Worksystem 4.5, Cambridge, MA) of a Coα_3[NMeIm]β[Im]-O_2 species. In the resulting minimized structures, a hydrogen bond distance of about 2.6−2.8 Å was found between the amide hydrogen and the terminal oxygen of the superoxide. A strong H-bonding interaction between the terminal electronegative oxygen and the amide is probably the driving force stabilizing the Co-superoxide core in our Co/Cu complexes. Similarly, in a recent structure of Co(T_{piv}PP)(NO_2)(1-MeIm), a H-bond was indicated between the amide of the picket fence and the oxygen of the nitrite,[77] which was found to point toward the amide hydrogen at a distance of 2.96 Å. Comparable H-bond interactions have been observed for other complexes such as Fe(T_{piv}PP) porphyrins, but to somewhat lesser extent because of electronic differences between the oxy states of the two metals. In heme-enzymes, H-bonding has been shown to occur between O_2 and distal residues, such as histidine, glutamine, or tyrosine. For example, a remarkable affinity for O_2, a factor of 10^4 higher than for mammalian Hb, was reported for Hb from the bloodworm *Ascaris*.[78] This effect is believed to originate from strong H-bonding between Tyr 30 to the terminal oxygen as well as between Gln 64 and the heme-bound oxygen. In the oxy forms of native and mutated (Co) myoglobin, the oxygen-distal histidine (His 64) distances range between 2.72 and 3.01 Å.[68,73]

Raman Spectroscopy. Raman spectra of the oxygenated [Co**4**] complex show a band at 1148 cm^{-1} that is not present in the non-oxygenated samples (Figure 7). This peak is isotopically sensitive and shifts to 1077 cm^{-1} upon $^{18}O_2$ substitution ($\Delta = 71$ cm^{-1}), which is indicative of ν(O−O) for cobalt-porphyrin-superoxide species.[4,5]

As depicted in Figure 8, Raman spectra of oxygenated [Co**4**Cu] show an isotope-sensitive band in the superoxide region at 1143 cm^{-1} that shifts to 1070 cm^{-1} upon $^{18}O_2$ substitution ($\Delta = 73$ cm^{-1}). Superoxide stretching frequen-

(75) Walker, F. A.; Bowen, J. *J. Am. Chem. Soc.* **1985**, *107*, 7632−7635.

(76) See Supporting Information.
(77) Jene, P. G.; Ibers, J. A. *Inorg. Chem.* **2000**, *39*, 3823−3827.
(78) Kloek, A. P.; Yang, J.; Mathews, F. S.; Goldberg, D. E. *J. Biol. Chem.* **1993**, *268*, 17669−17671.

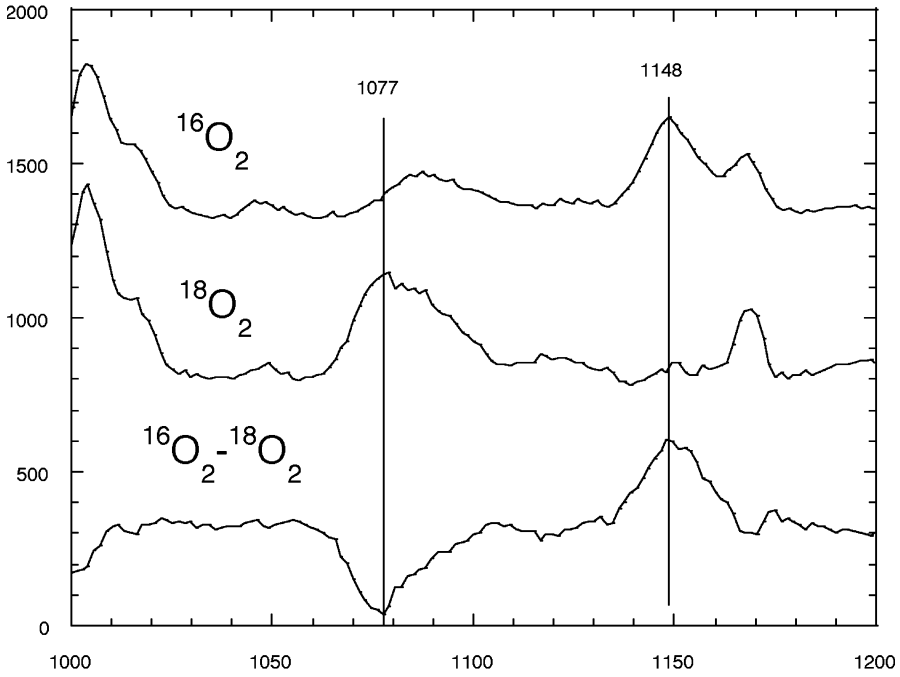

Figure 7. RR spectra of [Co**4**]O_2 with $^{16}O_2$ and $^{18}O_2$.

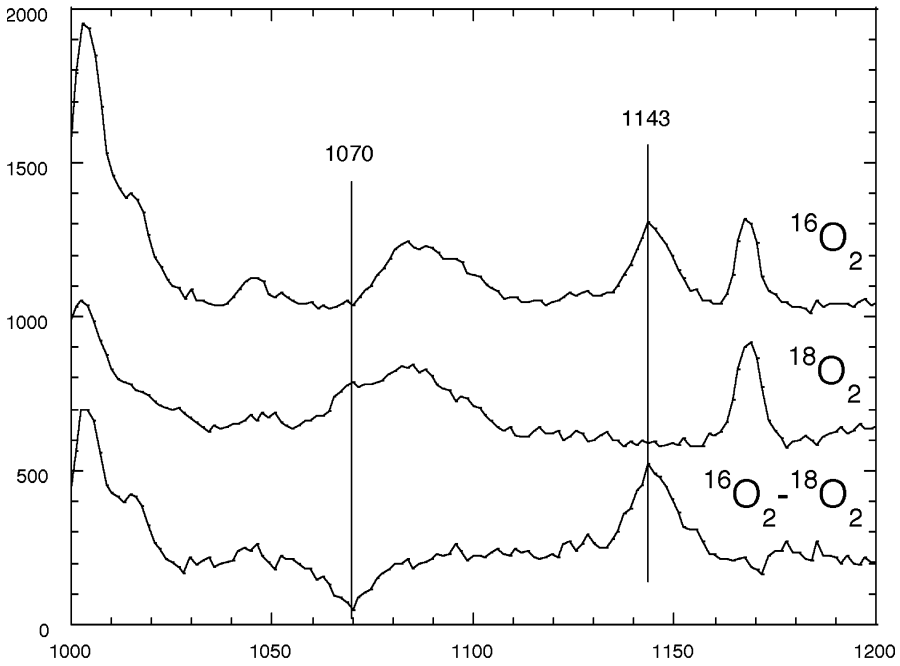

Figure 8. RR spectra of [Co**4**Cu]O_2 with $^{16}O_2$ and $^{18}O_2$.

cies for oxygenated [Co**4**Co] and [Co**4**Zn] species were found at 1147 cm^{-1} ($\Delta = 73$ cm^{-1}) and 1146 cm^{-1} ($\Delta = 72$ cm^{-1}), respectively, demonstrating the resemblance of the two systems. The notably lower ν(O−O) (1143 cm^{-1}) of the oxygenated [Co**4**Cu] complex indicates a slightly different environment for the superoxide species in Co/Cu, possibly because of differences in distal metal coordination geometry and/or charge.

The magnitudes of the measured isotope shifts were found to be ∼10% higher than the predicted shift of $\Delta = 65$ cm^{-1} for dioxygen alone. The reason for this difference is likely due to coupling with vibrational modes of the axial imidazole ligand as observed by Proniewicz et al.[79] Asymmetry of the $^{18}O_2$ peak indicates the potential for mode mixing with the broad peak at 1086 cm^{-1}, which would cause the $^{18}O_2$ superoxide peak to shift down in energy and lead to the unusually large isotope shift.

[TACN][PhIm] System. TACN superstructured Co porphyrins have previously been prepared,[17,18] and it was found that upon oxygenation the Co-only derivative binds O_2 reversibly, while the bimetallic TACN adduct forms a bridged Co−O_2−Cu peroxide complex, which undergoes

(79) Proniewicz, L. M.; Bruha, A.; Nakamoto, K.; Kyuno, E.; Kincaid, J. R. *J. Am. Chem. Soc.* **1989**, *111*, 7050−7056.

reduction of O_2 when 4 equiv of $Co(Cp)_2$ is added. For comparison to the present work, the [Co**5**] and [Co**5**Cu] porphyrins were synthesized and studied. In reaction of [Co**5**Cu] with O_2, Co superoxide was neither detected by EPR nor RR spectroscopy at any point during the course of the reaction. Consequently, we suggest that a Co−O_2−Cu adduct is formed. However, the observed bridged Cu(II) EPR signal could not be resolved from another Cu(II) signal which, after a day of reaction, was the only remaining EPR-active species. As evidenced by EPR, the final product consists of a Co(III)/Cu(II) couple (EPR-inactive cobalt). When the Co-only derivative was treated with oxygen, a reversible [Co**5**]O_2 (superoxide) adduct was confirmed by both spectroscopic techniques, yielding a RR ν(O−O) stretch at 1147 cm^{-1} (Δ = 73 cm^{-1}) and the characteristic Co-superoxide EPR signal at $g_\perp \sim 1.99$ and $g_\parallel \sim 2.07$ (Table 3). Contrary to the Co/Cu adduct, a cobalt superoxide is formed when treating [Co**5**Zn] with O_2, which was evidenced by EPR and RR spectroscopy (ν(O−O) = 1150 cm^{-1}; Δ = 73 cm^{-1}). Little change is observed between cobalt-porphyrin-superoxide stretching frequencies with different distal superstructures (TACN vs tris-imidazole). However, redox- versus non-redox-active distal metals may have a different influence on Co/O_2 chemistry as observed for the TACN-capped porphyrins.

Further Reactivity. After oxygenation, regardless of system, the Co-superoxide species in concentrated solutions were found to be stable. At RT under dry conditions, the Co-superoxide derivative stayed intact for as long as 10 days. Exposure to protons, from MeOH or acid, caused an immediate (<seconds) decomposition of the Co superoxide (which could explain the difficulty in observing Co-superoxide species by ESI-MS). The reduction of O_2 to $OOH^\bullet$/H_2O_2 is clearly promoted by protons.[80,81] The final stable product is EPR inactive suggesting a Co(III)−X species, where X denotes the corresponding base (MeO^-, Cl^-, Ac^-, OH^-, etc.). UV−vis spectra showed distinct changes in the Soret bands when the Co-superoxide complexes were treated with a variety of acids (HCl, HOAc, organic acid, etc.). Addition of base, such as aqueous sodium hydroxide, had no apparent effect on the decomposition of Co superoxide. With water present, the Co superoxide was less long-lived. Moreover, certain RR laser excitation wavelengths caused some disintegration of the Co-superoxide complex. This decomposition was most prominent for the Co-only porphyrins. Detailed analyses of these reactions were not undertaken.

Conclusions

A series of (P)Co(II) models with structural and chemical resemblance to the active site in C*c*O has been synthesized. Redox-active, oxyphilic Cu(I) or non-oxyphilic redox-stable metals (Ag(I) and Zn(II)) have been coordinated in the distal superstructure (tris-imidazole pickets), and the oxygenated products of both mono- and bimetallic porphyrins have been characterized by EPR, RR, and ESI-MS spectroscopy. Unexpectedly, Co superoxide was found to be the end product for all these porphyrin complexes. This is the first example of model compounds for C*c*O where two metals that readily react with dioxygen, placed at a favorable *inter*metallic distance, result in a metal-superoxide product rather than a metal−metal μ-peroxo or μ-oxo/hydroxo species. However, the distal metal in these models is not merely an innocent spectator. For the Co/Cu and Co/Zn porphyrins, H-bonding of the dioxygen unit to the picket-amide-NH is indicated by H/D EPR experiments. Negligible reversibility of O_2 binding is observed for all bimetallic porphyrins, whereas the Co-only porphyrins show reversible dioxygen binding. We propose that several factors, a tight distal cavity, H-bonding, and electrostatic effects, strongly influence the dioxygen affinity and the stabilization of bound superoxide. In comparison to native enzymes, the Co-only porphyrins resemble the Mb/Hb type of hemes (or CoMb/CoHb), where reversible superoxide formation is observed. However, the Co/Cu models show limited reversibility after oxygenation, thus approaching the nature of the active site of C*c*O. These results indicate that one possible role of Cu_B in C*c*O is to aid retention of O_2 and to stabilize a superoxide intermediate. Dioxygen binding kinetics, mechanistic studies, and electrochemistry of these Co porphyrins will be presented in a later publication.

Experimental Section

Materials and Methods. Reagents and solvents, purchased from Aldrich, Fluka, Alfa, Strem, or Lancaster, were of commercial reagent quality unless otherwise stated. Huenig base was stored over molecular sieves, and the SiO_2 and Al_2O_3 chromatography gels were used as received from EM Science. Under an inert atmosphere, tetrahydrofuran, benzene, and diethyl ether were distilled from sodium benzophenone ketyl while acetonitrile and dichloromethane were distilled from CaH_2 and methanol was distilled from magnesium prior to use. For NMR studies, $CDCl_3$ was vacuum transferred from 4 Å molecular sieves into flame-dried NMR tubes immediately prior to use. Synthesis of air-sensitive porphyrin compounds and all metalations were performed in a Vacuum Atmospheres glovebox (VAC) under a N_2 atmosphere with <1 ppm O_2 content. All porphyrin and metalloporphyrin NMR samples were prepared under an inert (N_2) atmosphere in 5 mm NMR tubes fitted with PTFE valves. RR, EPR, IR, and UV−vis samples were prepared in a glovebox. Oxygenations were performed via vacuum transfer of 100% $^{16}O_2$ (gas cylinder) or 100% $^{18}O_2$ (bulb) to samples (1 atm).

Instrumentation. All NMR spectra were recorded on a Varian Unity 500 MHz spectrometer. ^1H NMR spectra were referenced to residual protio-solvent signal, and ^{19}F NMR spectra were referenced to $CFCl_3$ (0 ppm). IR spectra were recorded on a Mattheson Infinity Series FTIR in a NaCl solution cell (path length 1.0 mm) of ~2 mM concentrations. EPR spectra were recorded on a Bruker EMX spectrometer (X-band) at 77 K in a 3 mm (o.d.) quartz tube fitted with a PTFE valve of analyte at millimolar concentration in glassified CH_2Cl_2. Data treatment and simulations of EPR spectra

(80) Steiger, B.; Anson, F. C. *Inorg. Chem.* **2000**, *39*, 4579−4585.
(81) Sawyer, D. T. *Oxygen Chemistry*; Oxford University Press: New York, 1991.
(82) Sorrell, T. N.; Jameson, D. L. *J. Am. Chem. Soc.* **1983**, *105*, 6013−6018.
(83) Sorrell, T. N.; Allen, W. E.; White, P. S. *Inorg. Chem.* **1995**, *34*, 952−960.
(84) Collman, J. P.; Berg, K. E.; Sunderland, C. J. Unpublished results.
(85) Hori, H.; Ikeda-Saito, M.; Yonetani, T. *J. Biol. Chem.* **1982**, *257*, 3636−3642.

were performed with the Bruker software packages XSophe, eprView, and WinEPR. UV−vis spectra were recorded on a Hewlett-Packard 8452A spectrometer at micromolar concentration. ESI-MS spectra were recorded on a Finnigan LCQ mass spectrometer at the PAN facility at Stanford University. FAB-MS spectra were measured by the Mass Spectrometry Facility at the University of California, San Francisco. Resonance Raman spectra were obtained using 458 nm Ar^+ (Coherent Sabre 25/7) ion lasers with incident power in the 5−25 mW range using a 135 backscattering arrangement. The scattered light was dispersed by a triple monochromator (Spex 1877 CP, equipped with 1200, 1800, and 2400 groove/mm gratings) and detected with a back-illuminated CCD camera (Princeton Instruments ST-135). Frozen solution samples in PTFE valve quartz NMR tubes were immersed in liquid nitrogen using an EPR finger dewar.

Synthesis. Synthesis of $H_2$1. Synthesis of H_2**1** was carried out according to an earlier description,[25] except for the two separate coupling reactions of imidazole and acetyl onto the distal and the proximal sides of the porphyrin, respectively. These two reactions are described in following paragraphs.

Coupling Reaction of Acetyl Chloride to H_2[TFA][NH_2] and Deprotection of the TFA. H_2[TFA][NH_2] (250 mg, 0.23 mmol) was dissolved in acetic acid (40 mL), and acetyl chloride (80 μL, 1.13 mmol) was added into the dark-purple solution, immediately rendering the solution dark-green. The reaction mixture was left stirring under nitrogen at RT in darkness for 3 h, whereupon a solution of NaOAc/HOAc (3.85 mL, 5 g anhyd NaOAc in 100 mL HOAc) was added slowly via syringe. CH_2Cl_2 (100 mL) was added into the reaction mixture, and the organic phase was extracted twice with 100 mL of distilled water and once with 100 mL dil $NaHCO_3$ (aq). After drying the organic phase with K_2CO_3, filtering, and evaporating the solvent, we obtained one major purple product (TLC: SiO_2; CH_2Cl_2 bubbled with NH_3). The crude H_2[TFA][Ac] was dissolved in 10 mL of CH_2Cl_2 followed by addition of 5 mL of a solution of MeOH prebubbled with NH_3(g) and cooled. The solution was left stirring for 1−2 days at RT in darkness. After evaporation of the solvent, the purple microcrystalline powder of H_2[NH_2][Ac] was purified by column chromatography using SiO_2 gel (230−400 mesh) and NH_3-bubbled CH_2Cl_2 as eluent. Yield: 144 mg (76%). ^{1}H NMR ($CDCl_3$, δ): 8.94−8.92 (6H, m, pyrrH), 8.78 (2H, d, pyrrH), 8.71 (1H, d, Ph_βH3), 7.98 (1H, d, Ph_βH6), 7.88 (2H, dd, $Ph_{\alpha2}$H3), 7.85−7.80 (2H, m, Ph_βH4, $Ph_{\alpha1}$H3), 7.64−7.61 (3H, td, $Ph_{\alpha2}$H6, $Ph_{\alpha1}$H6), 7.49 (1H, t, Ph_βH5), 7.21−7.16 (5H, m, $Ph_{\alpha2}$H4, $Ph_{\alpha1}$H4, αNH_2), 7.15−7.12 (5H, m, $Ph_{\alpha2}$H5, $Ph_{\alpha1}$H5, αNH_2), 6.75 (3H, s, αNH_2, NH_β), 3.60 (3H, s, $\beta COCH_3$), −2.66 (2H, s, porNH).

Coupling Reaction of *N*-Methyl-imidazole to H_2[NH_2][Ac]. H_2[NH_2][Ac] (100 mg, 0.12 mmol) was dissolved in a mixture of 50 mL of THF and 30 mL of acetonitrile, and *N*-methyl-imidazole acid chloride hydrochloride (227 mg, 1.2 mmol) was added under vigorous stirring at RT in darkness. Then, Huenig base (291 μL, 1.67 mmol) was added and the reaction monitored by TLC (SiO_2). The reaction was finished after stirring for about 1 h when one major spot, the least migrating one, was observed on the TLC plate. After quenching with distilled water, the aqueous phase was extracted with portions of CH_2Cl_2, and the combined organic phases washed once with a dil solution of $NaHCO_3$ (aq). The dichloromethane phase was dried over Na_2SO_4, filtered, and evaporated to dryness and the residual product of H_2**1** purified using a preparative TLC plate (SiO_2 1000 μm, CH_2Cl_2 saturated with NH_3(g) + 5% MeOH). Yield: 107 mg (86%). ^{1}H NMR ($CDCl_3$, δ): 8.93−8.78 (8H, m, pyrrH), 8.66 (1H, d, Ph_βH3), 8.57 (2H, d, $Ph_{\alpha2}$H3), 8.46 (1H, d, $Ph_{\alpha1}$H3), 8.13−8.11 (4H, m, $Ph_{\alpha2}$H6, $Ph_{\alpha1}$H6, NH_β), 8.01 (1H, d, Ph_βH6), 7.88 (3H, td, $Ph_{\alpha2}$H4, $Ph_{\alpha1}$H4), 7.84−7.81 (3H, m, Ph_βH4, $NH_{\alpha2}$), 7.64−7.60 (3H, m, $Ph_{\alpha2}$H5, $Ph_{\alpha1}$H5), 7.51(1H, t, Ph_βH5), 6.96 (1H, s, $Im_{\alpha1}$H2), 6.94 (2H, s, $Im_{\alpha2}$H2), 6.66 (1H, s, $NH_{\alpha1}$), 5.43 (3H, s, $Im_{\alpha1}$H4, $Im_{\alpha2}$H4), 3.62 (3H, s, $Im_{\alpha1}$CH3), 3.58 (6H, s, $Im_{\alpha2}$CH3), −2.56 (2H, s, porNH). ESI-MS: *m*/*z* 1041.5 $[(C_{61}H_{49}N_{14}O_4)]^+$ or H_2[NMeIm][Ac]$^+$ (100%). UV (toluene, 298 K) (λ, ϵ): 334 (44 × 10^3), 428 (257 × 10^3), 520 (21 × 10^3), 554 (7 × 10^3), 594 (7 × 10^3), 650 (4 × 10^3).

Synthesis of $H_2$2. As a combination of the descriptions in this paper and earlier work, this acetylamide-capped porphyrin was synthesized. The free base porphyrin together with its cobaltated complex are being reported and characterized here for the first time. ESI-MS: *m*/*z* $[C_{68}H_{52}F_3N_{10}O_4]^+$ 1129.4 (100%). ^{1}H NMR (DMSO, δ): 9.36 (s, 1H, $NH_{\alpha1}$), 9.11 (s, 2H, $NH_{\alpha2}$), 8.77−8.76 (m, 4H, pyrrH), 8.67−8.61 (m, 5H, Im_βH4, pyrrH), 8.10 (d, 1H, Ph_βH3), 8.05 (m, 3H, Ph_βH6, $Ph_{\alpha2}$H3), 7.88 (t, 1H, Ph_βH4), 7.85 (d, 2H, $Ph_{\alpha2}$H6), 7.81−7.77 (m, 3H, $Ph_{\alpha1}$H3, $Ph_{\alpha2}$H4), 7.72 (t, 1H, Ph_βH5), 7.67 (d, 1H, $Ph_{\alpha1}$H6), 7.54−7.50 (m, 4 H, $Ph_{\alpha2}$H5, $Ph_{\alpha1}$H4, $Ph_{\alpha1}$H5), 7.44 (s, 1H, NH_β), 7.13 (d, 2H, CF_3Ph-3,5-H), 6.95 (d, 2H, CF_3Ph-2,6-H), 6.84 (s, 1H, Im_βH2), 6.51 (s, 1H, benzoylH2), 6.44−6.41 (m, 2H, benzoylH5, benzoylH4), 6.21 (m, 1H, benzoylH6), 4.71 (s, 2H, benzoylCH_2), 1.28 (s, 3H, α-amideCH_3), 1.17 (s, 6H, α2-amideCH_3), −2.74 (s, 2H, porNH).

Synthesis of $H_2$3. Synthesis and characterization of H_2**3** has previously been reported in a paper by Collman et al.[25] Here, we only report the ESI-MS data as well as the 1H NMR assignment for comparison with other related porphyrins described in this paper. ESI-MS: *m*/*z* 1327.5 $[C_{77}H_{58}F_3N_{16}O_4]^+$ (100%). ^{1}H NMR ($CDCl_3$, δ): 8.92 (d, 2H, pyrrH), 8.90 (d, 2H, pyrrH), 8.87 (d, 2H, pyrrH), 8.84 (d, 2H, pyrrH), 8.80 (d, 1H, Ph_βH3), 8.53 (d, 2H, $Ph_{\alpha2}$H3), 8.42 (d, 1H, $Ph_{\alpha1}$H3), 8.10 (d, 1H, Ph_βH6), 8.10 (s, 1H, $NH_{\alpha1}$), 8.06 (d, 1H, $Ph_{\alpha1}$H6), 8.00 (d, 2H, $Ph_{\alpha2}$H6), 7.87−7.83 (m, 4H, Ph_βH4, $Ph_{\alpha1}$H4, $Ph_{\alpha2}$H4), 7.80 (s, 2H, $NH_{\alpha2}$) 7.61 (t, 1H, $Ph_{\alpha1}$H5), 7.57 (t, 1H, Ph_βH5), 7.54 (t, 1H, $Ph_{\alpha2}$H5), 7.45 (s, 1H, NH_β), 7.06 (d, 2H, CF_3Ph-3,5-H), 6.94 (s, 3H, $Im_{\alpha1}$H2, $Im_{\alpha2}$H2), 6.88 (s, 1H, Im_βH2), 6.80 (s, 1H, Im_βH4), 6.66 (d, 2H, CF_3Ph-2,6-H), 6.37 (s, 1H, benzoylH_2), 6.29 (t, 1H, benzoylH5), 6.28 (d, 1H, benzoylH4), 6.11 (d, 1H, benzoylH6), 5.41 (s, 2H, $Im_{\alpha2}$H4), 5.36 (s, 1H, $Im_{\alpha1}$H4), 4.11 (s, 2H, benzoylCH_2), 3.60 (s, 3H, $Me_{\alpha1}$), 3.58 (s, 6H, $Me_{\alpha2}$), −2.51 (s, 2H, porNH).

Synthesis of $H_2$4. Synthesis was carried out as described in a recent paper by Collman et al.[25]

Synthesis of $H_2$5. This triaza-cyclononane-capped porphyrin, H_2**5**, was prepared similarly to the reported α_3[TACN]β[Im] porphyrin.[24] These two porphyrin structures only differ by a phenyl ring on the proximal imidazole. Both proximal imidazole syntheses are reported in that same publication.

Porphyrin Metalation. [Co1]. In the glovebox, H_2**1** (23.5 mg, 0.02 mmol) and Co(II)$(OAc)_2\cdot 4H_2O$ (27 mg, 0.1 mmol) were slurried in freshly distilled THF (10 mL). The slurry was refluxed overnight and cooled, and the dark-red mixture had turned into a dark-orange solution. TLC (Al_2O_3; CH_2Cl_2/MeOH 95:5) showed two bright orange spots, which were assigned to be the mono- and bis-cobalt complexes of **1**. After evaporating the solvent, the product was redissolved in CH_2Cl_2 (3 mL) and extracted with an equal volume of aqueous EDTA solution (0.1 M) overnight to yield the mono-cobalt complex only. The organic phase was separated, dried over Na_2SO_4, filtered, and evaporated to dryness. A final small column chromatography on neutral Al_2O_3 was carried out using the elution system CH_2Cl_2/MeOH 95:5 giving orange microcrystals. Yield: 23.0 mg (93%). MS (FAB): *m*/*z* 1098.2 $[C_{61}H_{47}N_{14}O_4Co]^+$ (100%). EPR: see EPR section. UV (CH_2Cl_2, 298 K) (λ, ϵ): 414

(109×10^3), 534 (6×10^3) [+NMeIm = 416, 534; $+O_2$ = 436, 549].

[Co1Cu]. In the glovebox, [Co**1**] (6.4 mg, 6 μmol) was dissolved in dry THF (5 mL). A solution of 1 mol equiv of $Cu(I)PF_6(MeCN)_4$ in acetonitrile was prepared and slowly added to the clear orange-red solution of [Co**1**]. After stirring for a couple of hours, the reaction turned deeper red, and pentane was added to precipitate the Co−Cu complex. Filtration and drying of the product gave a tanned red compound. Yield: 7.3 mg (96%). ESI-MS: *m*/*z* 1162.6 $[(C_{61}H_{46}N_{14}O_4CoCu)]^+$ (100%). IR (CH_2Cl_2, cm^{-1}): ν(CuC−O) = 2085. *Caution: CO is toxic, and reactions should be performed in a well-ventilated fume hood*. UV (CH_2Cl_2, 298 K) (λ, ϵ): 412 (101×10^3), 534 (7×10^3) [+NMeIm = 416, 539; $+O_2$ = 436, 549].

[Co2]. In the glovebox, H_2**2** (3.0 mg, 2.5 μmol) and an excess of $Co(II)(OAc)_2 \cdot 4H_2O$ (approximately 5 mol equiv) were dissolved in freshly distilled THF (3 mL). The solution was left to stir overnight at RT whereupon the clear purple solution had turned into an orange-red solution. TLC (Al_2O_3; Bz/MeOH 90:10) showed only one bright orange spot and no further free-base porphyrin. After evaporating the solvent and running the product through a neutral Al_2O_3 column (Bz/MeOH 90:10), evaporation of the solvent gave an orange-red product of [Co**2**]. Yield: 3.6 mg (quantitative). MS: *m*/*z* 1185.3 $[(C_{68}H_{49}F_3N_{10}O_4Co)]^+$ (100%). EPR: see EPR section. UV(CH_2Cl_2, 298 K) (λ, ϵ): 413 (141×10^3), 533 (15×10^3) [$+O_2$ = 441, 556].

[Co3]. In the glovebox, H_2**3** (10.2 mg, 8 μmol) and an excess of $Co(II)(OAc)_2 \cdot 4H_2O$ (approximately 10 mol equiv) were dissolved in freshly distilled THF (5 mL). The reaction was left to reflux overnight and then cooled whereupon the purple-red solution had turned dark-orange. TLC (Al_2O_3; CH_2Cl_2/MeOH 95:5) showed two bright orange spots, a minor faster one and a major spot which were assigned to be the mono- and bis-cobalt complexes of **3**, respectively. After evaporating the solvent, the residue was redissolved in CH_2Cl_2 (2 mL) and extracted with an equal volume of aqueous EDTA solution (0.1 M) overnight to yield the mono-cobalt complex only. The organic phase was separated, dried over Na_2SO_4, filtered, and evaporated to dryness. Two column chromatography purifications were carried out, first on neutral Al_2O_3 (Bz/MeOH 90:10 → 80:20) and second on basic Al_2O_3 (Bz/MeOH 80:20) yielding red-orange microcrystals. Yield: 7.8 mg (73%). EPR: see EPR section. ESI-MS: *m*/*z* 1384.5 $[CoC_{77}H_{56}F_3N_{16}O_4]^+$ (100%). UV (CH_2Cl_2, 298 K) (λ, ϵ): 416 (188×10^3), 534 (11×10^3) [$+O_2$ = 436, 548].

[Co3Cu]. In the glovebox, [Co**3**] (2.1 mg, 1.5 μmol) was dissolved in THF (1 mL). A solution of 1 mol equiv of $Cu(I)PF_6(MeCN)_4$ in acetonitrile was slowly added to the clear red-orange solution of [Co**3**]. After a few hours of stirring at RT, the red Co/Cu complex was precipitated using pentane and isolated in quantitative yields (2.3 mg). EPR: see EPR section. ESI-MS: *m*/*z* 1446.3 $[CoC_{77}H_{56}F_3N_{16}O_4]^+$ (5%), 1483.1 $[CoC_{77}H_{55}F_3N_{16}O_4CuCl]^+$ (80%). IR (CH_2Cl_2, cm^{-1}): ν(Cu−C≡O) = 2082. *Caution: CO is toxic, and reactions should be performed in a well-ventilated fume hood*. UV (CH_2Cl_2, 298 K) (λ, ϵ): 414 (167×10^3), 536 (4×10^3) [$+O_2$ = 438 (177×10^3), 548 (12×10^3)].

[Co3]$^+$. To an NMR spectroscopy sample of [Co**3**] (2 mM, $CDCl_3$), approximately 1 mol equiv of PhNO was added to the solution under anaerobic conditions. A diamagnetic NMR spectrum was obtained after several hours. This reaction has demonstrated poor reproducibility with respect to producing a single product, and the reaction is currently under study. ^{1}H NMR ($CDCl_3$, δ): 9.13 (2H, d, pyrrH), 9.04 (3H, m, pyrrH, $Ph_{\alpha 1}$H3), 8.96 (6H, d, pyrrH, $NH_{\alpha 2}$), 8.75 (1H, d, Ph_βH3), 8.65 (4H, m, $Ph_{\alpha 2}$H3, $Ph_{\alpha 2}$H6), 8.14 (1H, d, $Ph_{\alpha 1}$H6), 7.87 (4H, m, Ph_βH6, $Ph_{\alpha 1}$H4, $Ph_{\alpha 2}$H4), 7.77 (1H, d, benzoylH6), 7.70 (3H, m, Ph_βH4, $Ph_{\alpha 2}$H5), 7.59 (1H, t, $Ph_{\alpha 1}$H5), 7.49 (1H, t, Ph_βH5), 7.37 (1H, s, NH_β), 7.15 (1H, s, $NH_{\alpha 1}$), 7.05 (5H, m, benzoylH5, CF_3Ph-3,5-H, $Im_{\alpha 2}$H2), 6.79 (1H, s, $Im_{\alpha 1}$H2), 6.45 (1H, d, benzoylH4), 5.70 (2H, CF_3Ph-2,6-H), 5.22 (2H, s, $Im_{\alpha 2}$H4), 4.11 (1H, s, $Im_{\alpha 1}$H4), 3.77 (6H, s, $Im_{\alpha 2}CH_3$), 3.63 (2H, s, benzoylCH_2), 3.60 (3H, s, $Im_{\alpha 1}CH_3$), 3.48 (2H, s, benzoylH2), 1.36 (1H, s, Im_βH4), 0.57 (1H, s, Im_βH2). ^{19}F NMR ($CDCl_3$, δ): −67.60 (s, 4.2 Hz); paramagnetic shift before oxidation −66.84 (s, 7.4 Hz).

[Co4]. In the glovebox, H_2**4** (6.2 mg, 4.3 μmol) and $Co(II)(OAc)_2 \cdot 4H_2O$ (approximately 5 mol equiv) were dissolved in dry THF (5 mL) and refluxed overnight. The solvent was evaporated, and the residue was dissolved in benzene (10 mL) and washed with water (5 mL). An overnight extraction of the benzene layer was carried out using 5 mL of an EDTA solution (0.1 M) followed by another 5 mL of water and finally drying of the benzene layer with Na_2SO_4(s). After evaporation of the solvent, the product was chromatographed first on neutral Al_2O_3 and then on basic Al_2O_3 (Bz/MeOH, 95:5) which after evaporation gave an orange-red product of [Co**4**]. Yield: 6.4 mg (quantitative). EPR: see EPR section. ESI-MS: *m*/*z* 1510.8 $[CoC_{86}H_{74}F_3N_{16}O_4]^+$ (100%), 756.5 $[CoC_{86}H_{75}F_3N_{16}O_4]^{2+}$ (20%). UV (CH_2Cl_2, 298 K) (λ, ϵ): 416 (181×10^3), 536 (12×10^3) [$+O_2$ = 443, 553].

[Co4Cu]. In the glovebox, [Co**4**] (3.2 mg, 2.1 μmol) was dissolved in dry THF (3 mL). Then, 1 mol equiv of $Cu(I)(PF_6)(MeCN)_4$ in acetonitrile was added, and the solution was left to stir for approximately 10 min upon which a slight color change was observed to darker red. The solvents were evaporated to dryness, and a red product was obtained. Yield: 3.6 mg (quantitative). EPR: see EPR section. ESI-MS: *m*/*z* 1573.6 $[CoC_{86}H_{73}F_3N_{16}O_4Cu]^+$ (100%), 1510.7 $[CoC_{86}H_{73}F_3N_{16}O_4]^+$ (65%). UV (CH_2Cl_2, 298 K) (λ, ϵ): 414 (202×10^3), 534 (5×10^3) [$+O_2$ = 430 (157×10^3), 544 (11×10^3)].

[Co4Zn]. In the glovebox, [Co**4**] (3.0 mg, 2.0 μmol) was dissolved in CH_2Cl_2/MeOH 80:20. A solution of 1 mol equiv of $Zn(II)(OAc)_2 \cdot 4H_2O$ in CH_2Cl_2/MeOH 80:20 was slowly added to the clear red-orange solution of [Co**4**] under vigorous stirring. After 3 h of stirring at RT, the solvent was evaporated and the pink-red Co/Zn complex isolated in quantitative yields (3.7 mg). EPR: see EPR section. UV (CH_2Cl_2, 298 K) (λ, ϵ): 415 (211×10^3), 533 (13×10^3) [$+O_2$ = 445, 559].

[Co4Ag]. In the glovebox, [Co**4**] (0.4 mg, 0.3 μmol) was dissolved in CH_2Cl_2/MeOH 80:20. A solution of 1 mol equiv of $Ag(I)PF_6$ in CH_2Cl_2/MeOH 80:20 was slowly added to the clear red-orange solution of [Co**4**] under vigorous stirring. After $^1/_2$ h of stirring at RT, the solvent was evaporated and the pink-red Co/Ag complex isolated in quantitative yields. *Note: Co(II)/Ag(I) is not stable overnight, even under dry conditions, because a redox reaction takes place most probably yielding the couple Co(III)/Ag(0). The Co(II)/Ag(I) sample had to be freshly made before each experiment.* EPR: see EPR section. ESI-MS: *m*/*z* 1653.4 $[CoC_{86}H_{73}F_3N_{16}O_4AgCl]^+$ (80%). UV (CH_2Cl_2, 298 K) (λ): 416, 540 [$+O_2$ = 437, 549].

[Co5]. In the glovebox, H_2**5** (5.5 mg, 4.5 μmol) and an excess of $Co(II)(OAc)_2 \cdot 4H_2O$ (approximately 10 mol equiv) were dissolved in 20% MeOH in THF (5 mL). The reaction was left to reflux overnight and then cooled to RT. After evaporating the solvent, the residue was redissolved in 5%MeOH/C_6H_6 (∼1−2 mL) and chromotographed (neutral Al_2O_3) with 10−30% MeOH/C_6H_6 gradient, as required to prompt elution. This affords the bimetallic $[Co\mathbf{5}Co]^{2+}$ species. Yield: 4.5 mg (69%). To [Co**5**Co] (3.5 mg, 2.4 μmol) in THF (2 mL) was added tetramethylethylenediamine

(2 drops) and the solution stirred for 1 h. The solvent was evaporated under reduced pressure and the residue dissolved in a minimum of C_6H_6. The solution was added to a neutral Al_2O_3 chromatography column, washed with C_6H_6, and eluted with 2% MeOH/C_6H_6. After evaporation of the eluent and drying under high vacuum 24 h, [Co**5**] was afforded. Yield: 2.8 mg (91%). EPR: see EPR section. ESI-MS: *m*/*z* 1283.4 $[CoC_{77}H_{66}N_{13}O_4]^+$ (100%). UV (CH_2Cl_2, 298 K) (λ, ϵ): 416 (188×10^3), 534 (11×10^3) [$+O_2$ = 436, 548].

[Co5Cu]. In the glovebox, [Co**5**] (1.68 mg, 1.31 μmol) was dissolved in THF (0.5 mL). A solution of 1 mol equiv of $(CuTf)_2 \cdot C_6H_6$ (290 μL of 11.3 mg Cu(I) in 10 mL MeCN) was added to the clear red-orange solution of [Co**5**] to rapidly precipitate a red solid. The suspension was diluted with 20% MeOH/THF (5 mL) and warmed to ensure dissolution. After filtration and evaporation, a quantitative yield of [Co**5**Cu]Tf was obtained. EPR: see EPR section. ESI-MS: *m*/*z* 1345.3 $[CoC_{76}H_{65}N_{13}O_4Cu]^+$ (20%), 1382.2 $[CoC_{76}H_{65}N_{13}O_4CuCl]^+$ (100%). IR (CH_2Cl_2, cm^{-1}): ν(Cu−C≡O) = 2096. *Caution: CO is toxic, and reactions should be performed in a well-ventilated fume hood.* UV (CH_2Cl_2, 298 K) (λ, ϵ): 414 (167×10^3), 536 (4×10^3) [$+O_2$ = 438 (177×10^3), 548 (12×10^3)].

[Co5Zn]. In the glovebox, [Co**5**] (2.30 mg, 1.52 μmol) was dissolved in THF (5 mL). A solution of 1 mol equiv of $ZnTf_2 \cdot H_2O$ (412 μL of 14.1 mg Cu(I) in 10 mL 5%MeOH/THF) was added to the clear red-orange solution of [Co**5**]. After 10 min, the solvent was evaporated under reduced pressure to provide a quantitative yield of [Co**5**Zn]Tf_2. EPR: see EPR section. ESI-MS: *m*/*z* 1345.3 $[CoC_{76}H_{65}N_{13}O_4ZnCF_3SO_3ClH_2O]^+$. UV ($CH_2Cl_2$, 298 K) ($\lambda$, ϵ): 414 (167×10^3), 536 (4×10^3) [$+O_2$ = 438 (177×10^3), 548 (12×10^3)].

Acknowledgment. The authors would like to thank STINT (The Swedish Foundation for International Cooperation in Research and Higher Education) (K.E.B.), the NSF (Grant CHE 9612725), and the NIH (Grant GM 17880-30) for financial support. Dr. G. Rombaut is gratefully acknowledged for help with Raman measurements, Mike Eubanks and Cindy Ginsberg, for preliminary work with **5**, and Adam Cole, for the preliminary crystallographic work presented in the Supporting Information. Thanks also to the Mass Spectrometry Facility at the University of California, San Francisco, for collection of FAB-MS.

Supporting Information Available: Full NMR, IR, and mass spectrometry spectra as well as crystallographic information for $Zn\alpha_4[NMeIm]Zn_2(OAc)_3(OH)$. This material is available free of charge via the Internet at http://pubs.acs.org.

IC020395I